2010 IEEE International Conference on Robotics and Automation
Anchorage Convention District
May 3-8, 2010, Anchorage, Alaska, USA

Control of Bipedal Running by the Angular-Momentum-Based Synchronization Structure

Keisuke Nakamura, Shigeki Nakaura, and Mitsuji Sampei

***Abstract*— This paper investigates the running control problem for the 7-link, 6-actuator planar bipedal robot including ankle joints. The control strategy is based on the "synchronization structure" with the angular momentum of the pivot point. The synchronization not only follows the simplified joint angle dynamics of human running but also generates the uniform running speed from wide range of initial speed, which claims that the controller is robust for the error of initial speed. Moreover, it successfully verifies the acceleration of running speed from 0.1[m/s], which is almost zero speed, to a uniform running speed "without" switching controllers. Finally, the controller is applied for the running on an uneven terrain, and it successfully achieves running with the maximum slope angle 6[deg], which is highly steep terrain in the real situation.**

I. Introduction

The control problem of human walking or running motion has many aspects such as impacts, phase jumps, state jumps, etc. and is widely examined. Several bipeds have already achieved the running motion such as ASIMO[1] manufactured by HONDA and HRP-2[2] developed by AIST. The controllers of those robots are based on Zero Moment Point stability criterion[3]. Other outstanding controllers are CPG based controllers [4], Passivity based controllers [5], Partial linearization approach with an optimal time trajectory[6], and Hybrid Zero Dynamics criterion with an optimal orbit [9].

Even though the large number of control strategies have been reported, the papers considering the efficiency of the ankle joints are few. Namely, ankle joints have been investigated to enlarge the set of stable region, not positively used for the running with high jumps or high speed. Moreover, the most of reported methods have not investigated the problem of running on uneven terrain with multiple link model.

The purpose of this paper is to investigate the running control problem for the 7-link, 6-actuator planar bipedal robot including ankle joints for positive use. In order to simplify the mathematical discussion of running motion, the dynamics of each joint angle in real human running is categorized into 3 dynamics patterns, and the proposed angular-momentum-based synchronization structure realizes those 3 different dynamics patterns simply.

K. Nakamura is with the Department of Mechenical and Control Engineering, Tokyo Institute of Technology, 2-12-1, O-okayama, Meguro-ku, Tokyo, 152-8552, Japan. nakamura@sc.ctrl.titech.ac.jp

S. Nakaura is with the Department of Mechanical Engineering, Sasebo National College of Technology, 1-1, Okishinmachi, Sasebo-shi, Nagasaki, 857-1193, Japan. nakaura@post.cc.sasebo.ac.jp

M. Sampei is with the Department of Mechenical and Control Engineering, Tokyo Institute of Technology, 2-12-1, O-okayama, Meguro-ku, Tokyo, 152-8552, Japan. sampei@ctrl.titech.ac.jp

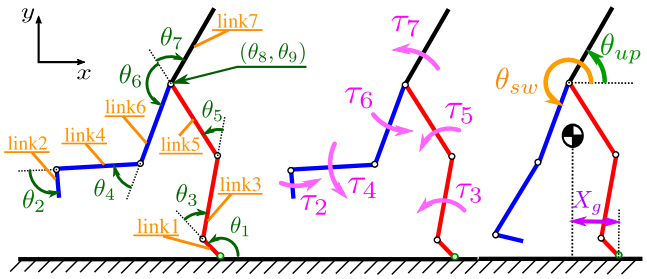

Fig. 1. 7-link planer biped model

In the validation, the synchronization realizes the acceleration from almost zero running speed to the uniform speed "without" switching controllers. The result also shows that the controller is robust for the error of initial running speed.

This paper also considers about the running on uneven terrain, and the controller successfully achieves the running motion with highly steep slopes.

II. Model and State Equations

A. Model of the Biped Robot

The running model treated in this paper is bipedal, and planar 7 rigid link model with (frictionless) revolute joints. The model is shown in Fig. 1. The support leg consists of link1 (foot), link3 (shin), and link5 (thigh), and the swing leg consists of link2 (foot), link4 (shin), and link6 (thigh). Link7 models the upper half body. The front edge of each foot is called a "toe" and the rear edge is called a "heel". The joint between the 2 legs and upper body is called a "hip", hereinafter, which represents the absolute position of the robot in the *x*-*y* coordinate. Configuration variables, input torques, and some additional variables used in this paper are explained in Table I. For the mathematical discussion, following two conditions are assumed.

A1) The friction between the robot's foot of the support leg and the ground is assumed to be large enough, so the contact point shall not slip during the contact.

A2) The foots do not have curvature, so the pivot point from heel to toe is discontinuously changed with an impact.

B. Phases for the Running Motion

For the running motion, three phases are defined depending on the pivot point of the robot. The schematic drawing of the three phases is shown in Fig. 2. The first phase is defined as "Flight Phase" when the robot floats in the air. The second phase is defined as "Stance Heel Phase" in which the robot sticks its heel on the ground. The third phase is defined as

TABLE I

PARAMETERS FOR THE BIPED MODEL

m_i	:	Mass of each link$i$ $(1 \leq i \leq 7)$
M	:	Total mass of the robot
l_i	:	Length of each link$i$ $(1 \leq i \leq 7)$
J_i	:	Moment of inertia of each link$i$ $(1 \leq i \leq 7)$
θ_1	:	Absolute angle of link1 from the ground
θ_i	:	Joint relative angle of each link$i$ $(2 \leq i \leq 7)$
(θ_8, θ_9)	:	Position of the hip in x-y coordinate
τ_i	:	Input torque at each joint
θ_{up}	:	Absolute angle of the upper body
θ_{sw}	:	Absolute angle of link6 (swing leg)
(X_g, Y_g)	:	Position of the center of mass (COM) of the robot from the ground contact (pivot) point
L_t	:	Angular momentum around the toe of link1
L_h	:	Angular momentum around the heel of link1
(x_t, y_t)	:	Position of the toe of the support leg
(x_h, y_h)	:	Position of the heel of the support leg
(X_{ga}, Y_{ga})	:	Absolute position of the COM of the robot
$\mu^*(x)$	:	Height of the ground at x
g	:	Acceleration of gravity

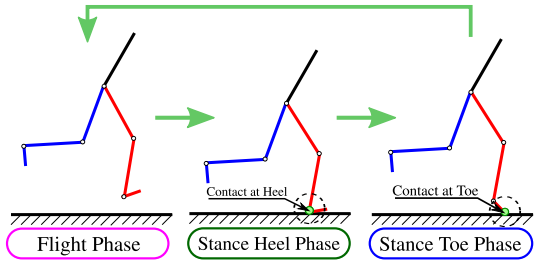

Fig. 2. Three phases for the bipedal running

"Stance Toe Phase" in which the robot sticks its toe on the ground. Additionally, the combined phase of Stance Heel Phase and Stance Toe Phase is defined as "Stance Phase". The robot achieves running motion by switching those phases and controllers. Following conditions hold in each phase.

- Flight Phase

BF-1) No ground contact point $(y_t > \mu^*(x_t), y_h > \mu^*(x_h))$

BF-2) The robot bends its ankle of the support leg sufficiently in this phase, so the switch from Flight Phase to Stance Toe Phase never happens.

- Stance Heel Phase

BSH-1) The robot sticks the support leg heel on the ground.

BSH-2) The ankle torque τ_3 is assumed to be zero so that the under-actuation degree is kept to be one.

- Stance Toe Phase

BST-1) The robot sticks the support leg toe on the ground.

Notice that the phase switch from Flight Phase to Stance Toe Phase is not investigated in this paper, which can be a future work for more efficient running.

For the phase switch, following conditions are assumed.

- From Flight Phase to Stance Heel Phase

CF-1) The switch occurs when $y_h \leq \mu^*(x_h)$.

CF-2) No impulse torque input is applied at impacts, so the angular velocity of each joint discontinuously jumps at each impact.

CF-3) The impact is perfectly inelastic collision.

- From Stance Heel Phase to Stance Toe Phase

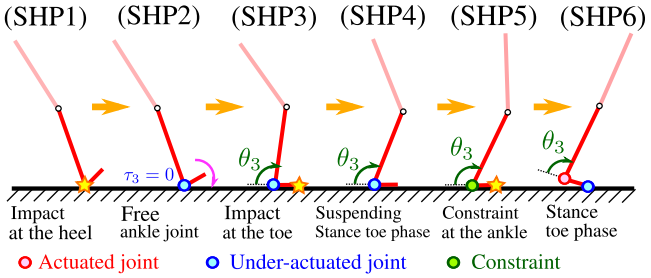

Fig. 3. Behavior of the ankle joint in Stance Heel Phase

CSH-1) The switch happens when $X_{ga} = x_t$.

CSH-2) The ankle joint of the support leg is assumed to be rigid at impacts for the simplicity, and other joint angular velocities jump by the impacts.

CSH-3) The impact is perfectly inelastic collision.

- From Stance Toe Phase to Flight Phase

CST-1) The switch happens when the ground contact force in the direction of y becomes less than zero.

The behavior of the ankle joint in Stance Heel Phase is shown in Fig. 3. First, the impact between Flight Phase and Stance Heel Phase occurs under the assumption of (CF-1),(CF-3), and (CF-3), which is described as (SHP1) in Fig. 3. Since $\tau_3 = 0$ in the phase, link1 falls on the ground with an impact at the toe (See (SHP2) and (SHP3) in Fig. 3). The impact in (SHP3) is also assumed to be perfectly inelastic collision. After the impact, $\tau_3 = 0$ holds until the condition (CSH-1) is satisfied, so the foot itself is stick to the ground ((SHP4) in Fig. 3). When (CSH-1) is satisfied, the ankle joint is fixed, and the impact at the toe occurs under the assumptions (CSH-2) and (CSH-3), which is (SHP5) in Fig. 3. Then, Stance Toe Phase starts ((SHP6) in Fig. 3).

C. Flight Phase Dynamics

In Flight Phase, the model has a distance from the ground, and the body is not constrained from the ground. Therefore, the state equation can be simply derived. Define configuration variables as $\boldsymbol{\theta}_f = [\theta_1, \cdots, \theta_9]^T \in \mathbb{R}^9$and define torque as $\boldsymbol{\tau}_f = [\tau_2, \cdots, \tau_7]^T \in \mathbb{R}^6$. Then, the Equation of Motion (EoM) is derived by Lagrange's method as

$$\boldsymbol{M}_f(\boldsymbol{\theta}_f)\ddot{\boldsymbol{\theta}}_f + \boldsymbol{C}_f(\boldsymbol{\theta}_f, \dot{\boldsymbol{\theta}}_f)\dot{\boldsymbol{\theta}}_f + \boldsymbol{G}_f(\boldsymbol{\theta}_f) = \boldsymbol{E}_f\boldsymbol{\tau}_f \quad , \qquad (1)$$

where $\boldsymbol{M}_f(\boldsymbol{\theta}_f) \in \mathbb{R}^{9\times9}$ is an inertia matrix, $\boldsymbol{C}_f(\boldsymbol{\theta}_f, \dot{\boldsymbol{\theta}}_f) \in \mathbb{R}^{9\times9}$ is a Coriolis matrix, $\boldsymbol{G}_f(\boldsymbol{\theta}_f) \in \mathbb{R}^9$ is a gravity term and $\boldsymbol{E}_f(\cdot) \in \mathbb{R}^{9\times6}$ shows the input coefficient matrix respectively. By selecting the state as $\boldsymbol{x}_f = [\boldsymbol{\theta}_f, \dot{\boldsymbol{\theta}}_f]^T$, (1) can be transformed into the following state equation.

$$\dot{\boldsymbol{x}}_f = \boldsymbol{f}_f(\boldsymbol{x}_f) + \boldsymbol{g}_f(\boldsymbol{x}_f)\boldsymbol{\tau}_f \qquad (2)$$

$$\boldsymbol{f}_f = \begin{bmatrix} \dot{\boldsymbol{\theta}}_f \\ \boldsymbol{M}_f^{-1}(\boldsymbol{C}_f\dot{\boldsymbol{\theta}}_f + \boldsymbol{G}_f) \end{bmatrix}, \quad \boldsymbol{g}_f = \begin{bmatrix} \boldsymbol{O}^{9\times6} \\ \boldsymbol{M}_f^{-1}\boldsymbol{E}_f \end{bmatrix}$$

D. Stance Toe Phase Dynamics

In addition to Flight Phase, the constraint at the pivot point has to be considered in Stance Toe Phase. With (A1) and

(BST-1), following constraint conditions can be derived:

$$\boldsymbol{N}_{st}(\boldsymbol{\theta}_f) = \begin{bmatrix} \theta_8 + l_1C_1 + l_3C_{13} + l_5C_{135} \\ \theta_9 + l_1S_1 + l_3S_{13} + l_5S_{135} \end{bmatrix} = \begin{bmatrix} 0 \\ 0 \end{bmatrix} \quad (3)$$

where $C_{ab\ldots} = \cos(\theta_a + \theta_b + \ldots)$, $S_{ab\ldots} = \sin(\theta_a + \theta_b + \ldots)$. Therefore, from (1) and (3), the EoM in Stance Toe Phase can be derived as follows.

$$\boldsymbol{M}_f\ddot{\boldsymbol{\theta}}_f + \boldsymbol{C}_f\dot{\boldsymbol{\theta}}_f + \boldsymbol{G}_f = \boldsymbol{E}_f\boldsymbol{\tau}_f + \boldsymbol{J}_{st}^T(\boldsymbol{\theta}_f)\boldsymbol{\lambda} \quad (4)$$

$$\boldsymbol{J}_{st}(\boldsymbol{\theta}_f)\dot{\boldsymbol{\theta}}_f = \boldsymbol{O}^{2\times 1} \quad (5)$$

$$\boldsymbol{J}_{st}(\boldsymbol{\theta}_f) = \partial \boldsymbol{N}_{st}(\boldsymbol{\theta}_f)/\partial\boldsymbol{\theta}_f \quad (6)$$

where $\boldsymbol{\lambda}$ is Lagrange's multiplier and is the generalized force which must be generated to maintain a constraint. Then, the EoM with the reduction of $(\theta_8, \theta_9, \dot{\theta}_8, \dot{\theta}_9)$ is represented as

$$\boldsymbol{M}_{st}(\boldsymbol{\theta}_{st})\ddot{\boldsymbol{\theta}}_{st} + \boldsymbol{C}_{st}(\boldsymbol{\theta}_{st}, \dot{\boldsymbol{\theta}}_{st})\dot{\boldsymbol{\theta}}_{st} + \boldsymbol{G}_{st}(\boldsymbol{\theta}_{st}) = \boldsymbol{E}_{st}\boldsymbol{\tau}_f \quad , \quad (7)$$

where $\boldsymbol{\theta}_{st} = [\theta_1, \cdots, \theta_7]^T \in \mathbb{R}^7$, $\boldsymbol{M}_{st}(\boldsymbol{\theta}_{st}) \in \mathbb{R}^{7\times 7}$is an inertia matrix, $\boldsymbol{C}_{st}(\boldsymbol{\theta}_{st}, \dot{\boldsymbol{\theta}}_{st}) \in \mathbb{R}^{7\times 7}$ is a Coriolis matrix, $\boldsymbol{G}_{st}(\boldsymbol{\theta}_{st}) \in \mathbb{R}^7$ is a gravity term, and $\boldsymbol{E}_{st}(\boldsymbol{\theta}_{st}) \in \mathbb{R}^{7\times 6}$ shows the input coefficient matrix. From (7), the state equation can be derived in the same process as Flight Phase.

E. Stance Heel Phase Dynamics

Same as Stance Toe Phase, the constraint at the pivot point always holds in Stance Heel Phase. Additionally, the behavior of the ankle joint in Fig. 3 must be considered.

1) Dynamics from (SHP1) to (SHP2) in Fig. 3: From (SHP1) to (SHP2) in Fig. 3, only the constraint at the ground contact point holds, so the constraint condition can be obtained as follows with the assumptions (A1) and (BSH-1).

$$\boldsymbol{N}_{sh1}(\boldsymbol{\theta}_f) = \begin{bmatrix} \theta_8 + l_3C_{13} + l_5C_{135} \\ \theta_9 + l_3S_{13} + l_5S_{135} \end{bmatrix} = \begin{bmatrix} 0 \\ 0 \end{bmatrix} \quad (8)$$

Same as (4) and (7) in Stance Toe Phase, the EoM and state equation from (SHP1) to (SHP2) can be determined with the change of $\boldsymbol{J}_{st}$ into $\boldsymbol{J}_{sh1} = \partial \boldsymbol{N}_{sh1}(\boldsymbol{\theta}_f)/\partial\boldsymbol{\theta}_f$.

2) Dynamics from (SHP3) to (SHP4) in Fig. 3: From (SHP3) to (SHP4) in Fig. 3, the constraint for sticking the foot on the ground needs to be considered at the toe in addition to (8). Therefore, following constraint condition can be derived.

$$\boldsymbol{N}_{sh2}(\boldsymbol{\theta}_f) = \begin{bmatrix} \theta_1 \\ \theta_8 + l_3C_{13} + l_5C_{135} \\ \theta_9 + l_3S_{13} + l_5S_{135} \end{bmatrix} = \begin{bmatrix} \text{const} \\ 0 \\ 0 \end{bmatrix} \quad (9)$$

The EoM is derived by the same process as (4), (5), (6), and (7), except the change of $\boldsymbol{J}_{st}$ into $\boldsymbol{J}_{sh2}(\boldsymbol{\theta}_f) = \partial \boldsymbol{N}_{sh2}(\boldsymbol{\theta}_f)/\partial\boldsymbol{\theta}_f$ (Here, $(\theta_1, \dot{\theta}_1)$ is reduced in addition to $(\theta_8, \theta_9, \dot{\theta}_8, \dot{\theta}_9)$).

3) Dynamics in (SHP5) in Fig. 3: At (SHP5) in Fig. 3, the assumption (CSH-2) is satisfied, so the ankle joint is fixed. Therefore, following constraint condition can be determined.

$$\boldsymbol{N}_{sh3}(\boldsymbol{\theta}_f) = \begin{bmatrix} \theta_3 \\ \theta_8 + l_3C_{13} + l_5C_{135} \\ \theta_9 + l_3S_{13} + l_5S_{135} \end{bmatrix} = \begin{bmatrix} \text{const} \\ 0 \\ 0 \end{bmatrix} \quad (10)$$

The EoM is derived by the same process as (4), (5), (6), and (7), except the change of $\boldsymbol{J}_{st}$ into $\boldsymbol{J}_{sh3}(\boldsymbol{\theta}_f) = \partial \boldsymbol{N}_{sh3}(\boldsymbol{\theta}_f)/\partial\boldsymbol{\theta}_f$ (Here, $(\theta_3, \dot{\theta}_3)$ is reduced in addition to $(\theta_8, \theta_9, \dot{\theta}_8, \dot{\theta}_9)$).

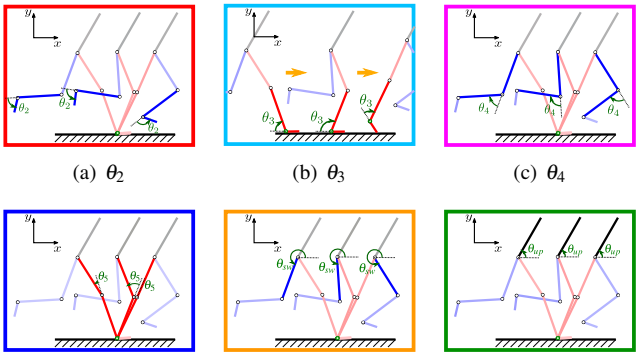

(a) θ_2 (b) θ_3 (c) θ_4

(d) θ_5 (e) θ_{sw} (f) θ_{up}

Fig. 4. Simplified behavior of each joint in Stance Phase

F. Impact Model

At impacts, variations of both states and inputs are small enough to be ignored compare to the constrained impulse $\boldsymbol{\lambda}_P$. Thereby, the EoM at an impact is represented as follows:

$$\boldsymbol{M}_f(\dot{\boldsymbol{\theta}}_+ - \dot{\boldsymbol{\theta}}_-) = \boldsymbol{J}^T(\boldsymbol{\theta}_f)\boldsymbol{\lambda}_P \quad , \quad \boldsymbol{J}(\theta_f)\dot{\boldsymbol{\theta}}_+ = \boldsymbol{O} \quad (11)$$

where $\dot{\boldsymbol{\theta}}_-$ is the generalized velocity just before an impact, and $\dot{\boldsymbol{\theta}}_+$ is the generalized velocity just after an impact.

$\boldsymbol{J}$ in (11) depends on the phase. Namely, $\boldsymbol{J}$ is substituted as $\boldsymbol{J}_{sh1}$ at the impact between Flight Phase and Stance Heel Phase, and $\boldsymbol{J}_{sh2}$ at the impact in (SHP3).

For the impact in (SHP5) in Stance Heel Phase, not the heel but the toe is fixed on the ground just after the moment of the impact. Therefore, $\boldsymbol{J} = \boldsymbol{J}_{sh4}$ is described as

$$\boldsymbol{N}_{sh4}(\boldsymbol{\theta}_f) = \begin{bmatrix} \theta_3 \\ \theta_8 + l_1C_1 + l_3C_{13} + l_5C_{135} \\ \theta_9 + l_1S_1 + l_3S_{13} + l_5S_{135} \end{bmatrix} = \begin{bmatrix} \text{const} \\ 0 \\ 0 \end{bmatrix} \quad (12)$$

$$\boldsymbol{J}_{sh4}(\boldsymbol{\theta}_f) = \partial \boldsymbol{N}_{sh4}(\boldsymbol{\theta}_f)/\partial\boldsymbol{\theta}_f \quad . \quad (13)$$

Then the generalized velocity just after an impact is derived from (11) as follows.

$$\dot{\boldsymbol{\theta}}_+ = \dot{\boldsymbol{\theta}}_- - \boldsymbol{M}_f^{-1}\boldsymbol{J}^T(\boldsymbol{J}\boldsymbol{M}_f^{-1}\boldsymbol{J}^T)^{-1}\boldsymbol{J}\dot{\boldsymbol{\theta}}_- \quad (14)$$

Also, the constraint impulse is represented by

$$\boldsymbol{\lambda}_P = (\boldsymbol{J}\boldsymbol{M}_f^{-1}\boldsymbol{J}^T)^{-1}\boldsymbol{J}\boldsymbol{M}_f^{-1}\dot{\boldsymbol{\theta}}_+ \quad . \quad (15)$$

III. Controller Design

This section proposes the controller based on a synchronization structure and confirms the validity.

A. Synchronization Design for Stance Phase

1) Categorization of Running Dynamics: In this paper, we consider only the simplified dynamics of running motion shown in Fig. 4 in order to simplify the synchronization structure. Here, the dynamics of the angle $(\theta_2, \theta_3, \theta_4, \theta_5, \theta_{sw}, \theta_{up})$ is specifically examined. The dynamics of each joint angle can be categorized into following three patterns.

D1) **Monotonically Increasing/Decreasing**
Namely, the angle is monotonically increasing or decreasing from an initial value during Stance Phase. The

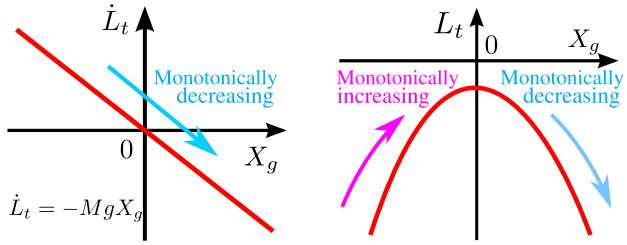

(a) $\dot{L}_t$ (b) L_t

Fig. 5. Behavior of L_t and $\dot{L}_t$ in Stance Phase

behavior can be seen at θ_2 and θ_{sw} which work as swing motions in order to proceed from the current step to the next. (See Fig. 4(a) for θ_2 and Fig. 4(e) for θ_{sw}.)

D2) **Switch Inc/Dec with a Max/Min Value**
Namely, the angle is firstly monotonically increasing/decreasing (Inc/Dec) and switches to be monotonically decreasing/increasing from a maximum/minimum (Max/Min) value. It physically means that the robot firstly bends the joint and extends the joint for the next jump. The behavior can be seen at θ_3, θ_4, and θ_5. (See Fig. 4(b) for θ_3, Fig. 4(c) for θ_4, and Fig. 4(d) for θ_5.)

D3) **Constant**
Namely, the angle is constant in Stance Phase. The behavior can be seen at θ_{up} (See Fig. 4(f) for θ_{up}).

In Section III-A.3, synchronization structure in Stance Phase is designed to realize these three patterns.

2) Synchronization Structure: In order to achieve the three patterns in Section III-A.1, the angular momentum around the ground contact point is specifically focused, which is L_h in Stance Heel Phase and L_t in Stance Toe Phase. Here, the characteristics of L_t are explained since L_h can be explained in the same discussion. From (7), L_t can be derived as

$$L_t = \boldsymbol{M}_{st1}(\boldsymbol{\theta}_{st})\dot{\boldsymbol{\theta}}_{st} \quad , \tag{16}$$

where $\boldsymbol{M}_{st1} \in \mathbb{R}^{1\times 7}$ is the first row vector of $\boldsymbol{M}_{st} \in \mathbb{R}^{7\times 7}$. Namely, $\boldsymbol{M}_{st} = [\boldsymbol{M}_{st1}^T, *]^T$. In fact, L_t is the generalized momentum conjugate to the cyclic variable and is shown to be relative degree 3 in [7]. Therefore, $\dot{L}_t$ is relative degree 2. $\dot{L}_t$ is described as follows.

$$\dot{L}_t = \boldsymbol{M}_{st1}(\boldsymbol{\theta}_{st})\ddot{\boldsymbol{\theta}}_{st} + \boldsymbol{C}_{st1}(\boldsymbol{\theta}_{st}, \dot{\boldsymbol{\theta}}_{st})\dot{\boldsymbol{\theta}}_{st} = -MgX_g \quad , \tag{17}$$

where $\boldsymbol{C}_{st1} \in \mathbb{R}^{1\times 7}$ is the first row vector of $\boldsymbol{C}_{st} \in \mathbb{R}^{7\times 7}$ in (7). Therefore, $\dot{L}_t$ is monotonically decreasing while X_g is monotonically increasing. The relationship between $\dot{L}_t$ and X_g is schematically shown in Fig. 5(a). Since X_g is the position of the COM of the robot in x direction, X_g is ensured to be monotonically increasing during running motion.

From (17), $\dot{L}_t = 0$ when $X_g = 0$. $X_g = 0$ means that the COM of the robot is in the upright position of the ground contact point, which normally occurs in Stance Phase. Therefore, L_t is increasing and is decreasing from a maximum value at $X_g = 0$ (See Fig. 5(b)).

The key idea of the synchronization structure is to use the behavior of L_t and $\dot{L}_t$ in Stance Phase to realize the three dynamics pattern (D1)-(D3). Namely, the dynamics pattern (D1) is similar to the behavior of $\dot{L}_t$ in Stance Phase, and (D2) is similar to the behavior of L_t. Thus, the dynamics (D1) and (D2) can be realized by making each joint angle synchronize with $\dot{L}_t$ and L_t. Therefore, the synchronization structure is represented as follows.

E1) **Synchronization between $\dot{L}_t$ (or $\dot{L}_h$) and θ_i**
➪ The pattern (D1) is realized for θ_2 and θ_{sw}.

E2) **Synchronization between L_t (or L_h) and θ_i**
➪ The pattern (D2) is realized for θ_3, θ_4 and θ_5.

E3) **No synchronization (Functions of only θ_i)**
➪ The pattern (D3) is realized for θ_{up}.

The synchronization can be achieved by designing a first order linear function. For example, if

$$y_{ex} = K_{ex1}L_t - (\theta_{ex} + K_{ex2}) \tag{18}$$

is zeroed, θ_{ex} is synchronized with L_t including a scaling factor K_{ex1} and a bias K_{ex2}.

3) Synchronization Structure Design: In consideration of (E1)-(E3) in Section III-A.2, following synchronized functions are designed for Stance Phase.

- **Stance Toe Phase**

$$\begin{bmatrix} y_2 \\ y_3 \\ y_4 \\ y_5 \\ y_{sw} \\ y_{up} \end{bmatrix} = \begin{bmatrix} K_{\theta_2 st}\dot{L}_t - (\theta_2 - K_{2st}) \\ K_{\theta_3 st}(L_t - L_{ti} - K_{3st}) - (\theta_3 - \theta_{3i}) \\ K_{\theta_4 st}(L_t - L_{ti} - K_{4st}) - (\theta_4 - \theta_{4i}) \\ K_{\theta_5 st}(L_t - L_{ti} - K_{5st}) - (\theta_5 - \theta_{5i}) \\ K_{\theta_{sw} st}\dot{L}_t - (\theta_{sw} - K_{swst}) \\ \theta_{up} - K_{upst} \end{bmatrix} , \tag{19}$$

where L_{ti} is the initial value of L_t in Stance Toe Phase, and θ_{3i}, θ_{4i}, and θ_{5i} represent the initial values of θ_3, θ_4, and θ_5 in Stance Toe Phase, respectively. For the pattern (E2), the offset of both L_t and θ is taken so that the value of the function is close to be zero for the synchronization.

$(K_{\theta_2 st}, K_{\theta_3 st}, K_{\theta_4 st}, K_{\theta_5 st}, K_{\theta_{sw} st})$ is the scaling factor of the synchronization, and $(K_{2st}, K_{3st}, K_{4st}, K_{5st}, K_{swst})$ is the bias term. The absolute angle of the upper body is set as K_{upst}.

- **Stance Heel Phase**

Basically, the synchronized functions in Stance Toe Phase are used for Stance Heel Phase, so y_2, y_{sw}, and y_{up} are used for Stance Heel Phase with the change of L_t into L_h. There are two different points of the functions from Stance Toe Phase. First, τ_3 is assumed to be zero in Stance Heel Phase, so y_3 in (19) is not considered. Second, the functions with respect to L_t, namely y_4 and y_5, work for bending the robot's knees in Stance Heel Phase. Since $(K_{\theta_4 st}, K_{\theta_5 st})$ is quite big scaling factor for its high jump in Stance Toe Phase, the same parameter $(K_{\theta_4 st}, K_{\theta_5 st})$ for Stance Heel Phase bends its knees too much. Therefore, different scaling factors and biases are used for Stance Heel Phase. Hence, the new scaling factors and bias terms are described as follows.

$$\begin{bmatrix} y_4 \\ y_5 \end{bmatrix} = \begin{bmatrix} K_{\theta_4 sh}(L_h - L_{hi}) - (\theta_4 - K_{4sh}) \\ K_{\theta_5 sh}(L_h - L_{hi}) - (\theta_5 - K_{5sh}) \end{bmatrix} , \tag{20}$$

where L_{hi} is the initial value of L_h.

- **Other Features**

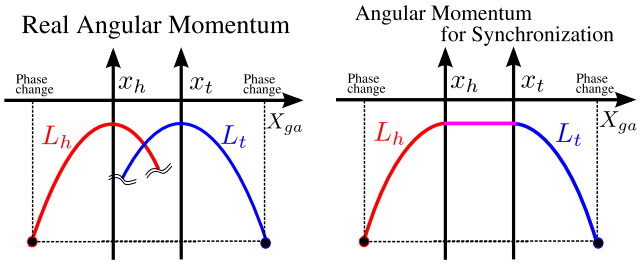

(a) Real L_t and L_h (b) Complemented L_t and L_h

Fig. 6. L_t, L_h, and the angular momentum for synchronization

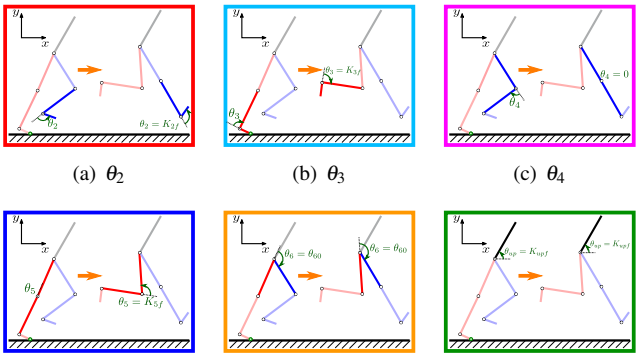

(a) θ_2 (b) θ_3 (c) θ_4

(d) θ_5 (e) θ_{sw} (f) θ_{up}

Fig. 7. Simplified behavior of each joint in Flight Phase

Since L_t and L_h has their maximum values in different x, namely x_t and x_h, the synchronization with both L_t and L_h has two maximum values in Stance Phase (See Fig. 6(a)). It means that the robot's knees bend two times in Stance Phase, which is not a desired motion. To solve the problem, synchronized functions which is different from y_3 and y_4 is designed in order to connect the two maximum values of L_t and L_h (See Fig. 6(b)). Therefore,

$$\begin{bmatrix} y_4 \\ y_5 \end{bmatrix} = \begin{bmatrix} \theta_4 - K_{4sh} \\ \theta_5 - K_{5sh} \end{bmatrix} \tag{21}$$

is used when $x_h \leq X_{ga} \leq x_t$.

B. Synchronization Design for Flight Phase

1) Categorization of Running Dynamics: Same as Section III-A.1, the behavior of each joint angle in Flight Phase is simplified and is shown in Fig. 7. Here, the dynamics of the angle $(\theta_2, \theta_3, \theta_4, \theta_5, \theta_{sw}, \theta_{up})$ is examined. For the controller design, following simple behavior is considered.

F1) The ankle joints of both legs are bent before landing.
➪ θ_2 and θ_3 are fixed at desired angles.(Fig. 7(a) (b))

F2) The knee of the landing leg is extended before landing in order to reduce an impact shock.
➪ θ_4 is fixed close to 0 [deg](See Fig. 7(c)).

F3) The knee of the hind leg is bent before landing.
➪ θ_5 is fixed at a desired angle (See Fig. 7(d)).

F4) The absolute angle of link6 and link7 are constant.
➪ θ_{sw} and θ_{up} are fixed (See Fig. 7(e) and Fig. 7(f)).

2) Synchronization Structure Design: In order to achieve (F1)-(F4) in Flight Phase, following functions are designed.

$$\boldsymbol{y}_f = \begin{bmatrix} y_2 \\ y_3 \\ y_4 \\ y_5 \\ y_{sw} \\ y_{up} \end{bmatrix} = \begin{bmatrix} \theta_2 - K_{2f} \\ \theta_3 - K_{3f} \\ \theta_4 - K_{4f} \\ \theta_5 - K_{5f} \\ \theta_{sw} - K_{swf} \\ \theta_{up} - K_{upf} \end{bmatrix}, \tag{22}$$

where $(K_{2f}, K_{3f}, K_{4f}, K_{5f}, K_{swf}, K_{upf})$ is designed parameter. In fact, no synchronization is used here since the angular momentum is not defined with respect to the pivot point.

C. Input-Output Linearization and Synchronization

This section briefly explains Input-Output linearization [11]. Here, only Flight Phase is examined, but the linearization in Stance Phase can be explained in the same discussion.

The synchronized functions designed in Section III-A.3 and Section III-B.2 have the relative degree 2. Therefore, the inputs for synchronization is obtained in following form.

$$\boldsymbol{\tau}_f = \begin{bmatrix} L_{g_f} L_{f_f} h_1 \\ \vdots \\ L_{g_f} L_{f_f} h_6 \end{bmatrix}^{-1} \left(\boldsymbol{v} - \begin{bmatrix} L_{f_f}^2 h_1 \\ \vdots \\ L_{f_f}^2 h_6 \end{bmatrix} \right), \tag{23}$$

where $\boldsymbol{h} = [h_1, h_2, h_3, h_4, h_5, h_6]^T = \boldsymbol{y}_f$, $\boldsymbol{v}$ is a new input described as $\ddot{\boldsymbol{y}}_f = \boldsymbol{v}$. Here, $\boldsymbol{v}$ is derived using LQR control.

D. Numerical Validation

This section confirms the numerical validation. Physical parameters are shown in Table II, and other parameters related to synchronized functions are set as Table III, where θ_{swi} is the initial value of θ_{sw} in Flight Phase.

The behavior of running speed $\dot{X}_{ga}$ is shown in Fig. 8. In the figure, the results with 5 different initial running speed are shown with the same parameters. As seen in the result, the final values are the same, which means that the controller is robust for the error of the initial value of $\dot{X}_g$.

In Fig. 9, the simulation result with the initial running speed $\dot{X}_g = 0.4$[m/s] is shown. At the first step, the speed becomes about $\dot{X}_g = 0.1$[m/s], and the controller successfully accelerates the speed. Note that there is no controller switch for the motion, and it adapts for wide range of running speed, which is one of the advantages of the controller.

IV. Running on an Uneven Terrain

The terrain considered in this paper is schematically shown in Fig. 12. The ground consists of 1.2[m] length blocks, and each block has each different slope angle μ_j[rad], where j is an index number. μ_j is randomly obtained as follows.

$$\mu_j = 2A_{max}(\text{rand}() - 0.5)(\pi/180), \tag{24}$$

where A_{max}[deg] is the maximum slope angle, and rand() is the uniform random number which is $0 \leq \text{rand}() \leq 1$. Fig. 10 shows the simulation result on an uneven terrain with $A_{max} = 6$[deg]. The parameters of the controller are exactly the same as Table III. The result successfully verifies the

TABLE II

PHYSICAL PARAMETERS

m_1	0.5 [kg]	l_1	0.10 [m]	J_1	$\frac{m_1 l_1^2}{12}$
m_2	0.5 [kg]	l_2	0.10 [m]	J_2	$\frac{m_2 l_2^2}{12}$
m_3	2.0 [kg]	l_3	0.30 [m]	J_3	$\frac{m_3 l_3^2}{12}$
m_4	2.0 [kg]	l_4	0.30 [m]	J_4	$\frac{m_4 l_4^2}{12}$
m_5	5.0 [kg]	l_5	0.30 [m]	J_5	$\frac{m_5 l_5^2}{12}$
m_6	5.0 [kg]	l_6	0.30 [m]	J_6	$\frac{m_6 l_6^2}{12}$
m_7	15.0 [kg]	l_7	0.30 [m]	J_7	$\frac{m_7 l_7^2}{12}$

TABLE III

PARAMETERS FOR SYNCHRONIZED FUNCTIONS

$K_{\theta_2 st}$	$-0.5\pi/180$	K_{2st}	$95\pi/180$	$K_{\theta_3 st}$	$\frac{-30}{1.1}\frac{\pi}{180}$	K_{3st}	1
$K_{\theta_4 st}$	$\frac{-30}{1.1}\frac{\pi}{180}$	K_{4st}	1	$K_{\theta_5 st}$	$\frac{25}{1.1}\frac{\pi}{180}$	K_{5st}	1
$K_{\theta_{sw} st}$	$-\frac{14}{40}\frac{\pi}{180}$	K_{swst}	$260\pi/180$			K_{upst}	$80\pi/180$
$K_{\theta_4 sh}$	-0.05	K_{4sh}	$-110\pi/180$	$K_{\theta_5 sh}$	-0.05	K_{5sh}	$35\pi/180$
K_{2f}	$110\pi/180$	K_{3f}	$-110\pi/180$	K_{4f}	0	K_{5f}	$80\pi/180$
K_{swf}	$-\theta_{swi}$	K_{upf}	$80\pi/180$				

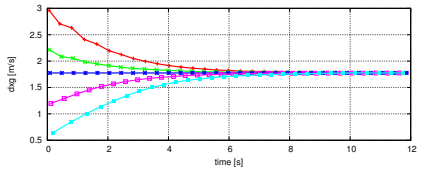

Fig. 8. Comparison of $\dot{X}_g$ with the change of the initial speed

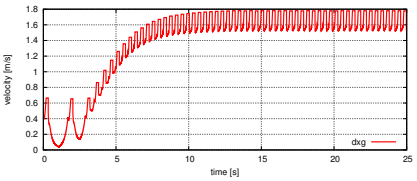

Fig. 9. Acceleration of $\dot{X}_g$ from 0.1[m/s]

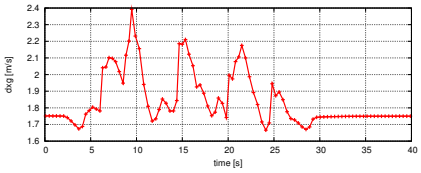

(a) Behavior of $\dot{X}_g$

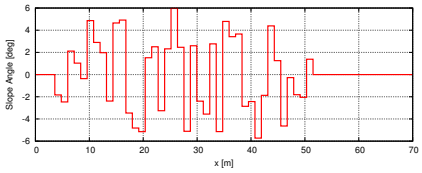

(b) Slope angle

Fig. 10. Running on a random terrain when $A_{\max} = 6$[deg]

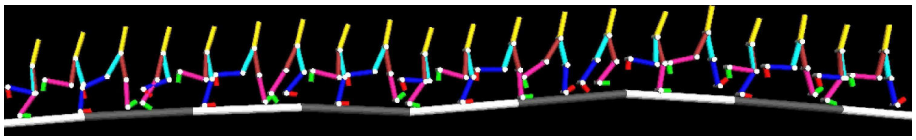

Fig. 11. Snapshots of running on uneven terrain ($A_{max} = 6$[deg])

motion. Fig. 11 shows the snapshots of the running with $A_{max} = 6$[deg]. Finally, the running motion on the terrain with the maximum angle 6[deg] is successfully verified.

V. CONCLUSION

In this paper, the running control for the 7-link, 6-actuator planar biped including ankle joints is specifically examined.

Firstly, a model of the bipedal robot was determined in consideration of the constraints, impacts, and assumptions observed in a real running motion. For the controller design, the angular-momentum-based synchronization structure was proposed, whose design is based on the simplified dynamics patterns of each joint angle in real human running.

In the numerical validation, it was shown that the controller was robust for the error of initial value of the running speed. Also, the acceleration of running speed from almost zero speed to a uniform speed was achieved.

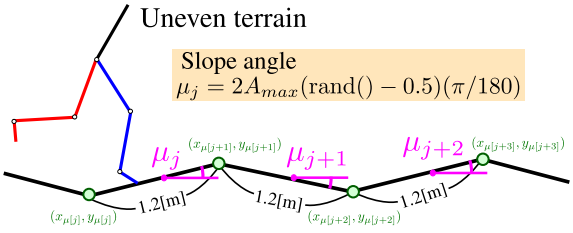

Fig. 12. Uneven terrain considered

In addition, the same controller successfully achieves the running motion on an uneven terrain with the maximum slope angle 6[deg]. Note that no switch controllers is required, which is the advantage of this controller.

REFERENCES

[1] (2009, Sep.), Honda Worldwide - ASIMO [Online]. Available: http://world.honda.com/ASIMO/

[2] (2009, Sep.), Humanoid Robotics Group Intelligent Systems Institute AIST [Online]. Available: http://www.is.aist.go.jp/humanoid/index.html

[3] S. Kajita, T. Nagasaki, K. Kaneko, H. Hirukawa, "ZMP-Based Biped Running Control," *IEEE Robotics and Automation Magazine*, vol. 14, no. 2, pp. 63–72, Jun. 2007.

[4] N. Sadati, K. Hamed, "CPG Based Controller for a 5-Link Planar Biped Robot," in *Proc. of IEEE ICM2007*, May. 2007, pp. 1–6.

[5] M. W. Spong, F. Bullo, "Controlled symmetries and passive walking," *IEEE Trans. on Autom. Control*, vol. 50, no. 7, pp. 1025–1031, 2005.

[6] S. Celikovsky, J. Zikmund, C. Moog, "Partial exact linearization design for the Acrobot walking," in *Proc. of American Control Conference*, Jun. 2008, pp. 874–879.

[7] J. W. Grizzle, C. H. Moog, C. Chevallereau, "Nonlinear control of mechanical systems with an unactuated cyclic variable," *IEEE Trans. on Autom. Control*, vol. 50, no. 5, pp. 559–576, May. 2005.

[8] E. R. Westervelt, J. W. Grizzle, and D. E. Koditschek, "Hybrid zero dynamics of planar biped walkers," *IEEE Trans. Autom. Control*, vol. 48, no. 1, pp. 42–56, Jan. 2003.

[9] C. Chevallereau, E. R. Westervelt, and J. W. Grizzle, "Asymptotically stable running for a five-link, four-actuator, planar bipedal robot," *Int. J. of Robotics Research*, vol. 24, no. 6, pp. 431–464, Jun. 2005.

[10] T. Shimizu, S. Nakaura, and M. Sampei, "The Control of a Bipedal Running Robot based on Output Zeroing considered Rotation of the Ankle Joint," in *Proc. the 45th IEEE Conf. Dec. Control*, San Diego, USA, Dec. 2006, pp. 6456–6461.

[11] A. Isidori, *Nonlinear Control Systems*, 3rd Ed., Berlin, Germany: Springer-Verlag, 1995.